RSC Advances

PAPER

View Article Online
View Journal | View Issue

Cite this: *RSC Adv.*, 2020, **10**, 37749

SiO_2@MnO_x@Na_2WO_4@SiO_2 core–shell-derived catalyst for oxidative coupling of methane†

La-Hee Park,[ab] Ye Rim Jo,[a] Jae-Wook Choi,[a] Dong Jin Suh,[ab] Kwang Ho Song[bc] and Jeong-Myeong Ha*[abd]

Received 9th June 2020
Accepted 3rd October 2020

DOI: 10.1039/d0ra05081d

rsc.li/rsc-advances

SiO_2@MnO_x@Na_2WO_4@SiO_2 core–shell catalysts were prepared and their fabrication was confirmed using transmission electron microscopy. The formation of Mn-based nanosheets on the silica spheres is important for the deposition of nanoscopic Na_2WO_4. The SiO_2@MnO_x@Na_2WO_4@SiO_2 core–shell catalysts were used for the oxidative coupling of methane at a temperature of 700–800 °C at which the nanostructures were completely destroyed. Although the core–shell structures did not survive the high-temperature oxidative coupling of methane, the selective production of olefins and paraffins can be attributed to highly dispersed Na_2WO_4 derived from confined core–shell structures.

1. Introduction

Methane is a major component of natural gas and potential feedstock for the production of chemicals and fuels.[1,2] While it is a building block for the preparation of many complex organic chemicals, the conversion of stable C–H bonds is difficult. Methane can be indirectly transformed into larger organic molecules *via* synthesis gas.[3] It can also be directly converted into functionalized building blocks including methanol,[4] methyl halides,[5] and ethylene.[6] Oxidative coupling of methane (OCM) to paraffins and olefins has attracted much interest because of its high productivity.[3,7,8] Because catalysts are important for the determination of the efficiency of OCM, many catalysts have been suggested for the development of economically feasible processes.[7,9,10]

Several metal oxide catalysts including perovskites,[11,12] metal oxide nanoparticles,[13] and other mixed metal oxides[14] have been proposed for the active and selective OCM process. One of the most efficient OCM catalysts,[15] Na_2WO_4/Mn/SiO_2 can be fabricated by depositing Na_2WO_4 and Mn on an SiO_2 support. Although the reaction mechanism is still controversial,[9] it has been suggested that Na_2WO_4 and Mn act as active component and promoter, respectively.[9,16,17] Scientists attempted to improve the Na_2WO_4/Mn/SiO_2 catalyst by adding promoters[16,18,19] and modifying the support,[20] but nanostructured Na_2WO_4/Mn/SiO_2 has not been used because of the high OCM reaction temperature.

In this study, core–shell structures composed of Na_2WO_4–Mn–SiO_2 were prepared as precursors of OCM catalysts (Scheme 1). Based on the active or selective catalysis using core–shell structures reported in the literature,[21,22] the objectives of building a core–shell structure are the (i) dispersion of Na_2WO_4 and Mn on the silica surface, (ii) stabilization of Na_2WO_4 and Mn components at the high reaction temperatures of 700–900 °C, and (iii) formation of possible Na_2WO_4, Mn, and SiO_2 complexes to achieve an improved catalytic activity. Particularly, an outer shell of SiO_2 was added to immobilize Na_2WO_4 and MnO_x shells at the high reaction temperature and to potentially prepare a highly dispersed mixture of Na_2WO_4, MnO_x, and silica which could improve the catalytic activity. By using the highly dispersed Na_2WO_4 of the core–shell precursors, the selective formation of ethane and ethylene is favored compared with the bulk Na_2WO_4/Mn/SiO_2 catalyst, which allows the deep oxidation to CO_2. While well-defined core–shell structures cannot survive

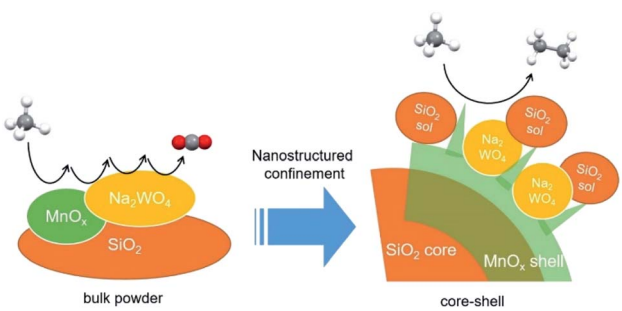

Scheme 1 Methane activation using core–shell catalysts.

[a]*Clean Energy Research Center, Korea Institute of Science and Technology, Seoul 02792, Republic of Korea. E-mail: jmha@kist.re.kr*

[b]*Graduate School of Energy and Environment (Green School), Korea University, Seoul 02841, Republic of Korea*

[c]*Department of Chemical and Biological Engineering, Korea University, Seoul 02841, Republic of Korea*

[d]*Division of Energy and Environment Technology, KIST School, Korea University of Science and Technology, Seoul 02792, Republic of Korea*

† Electronic supplementary information (ESI) available. See DOI: 10.1039/d0ra05081d

at high OCM reaction temperatures, they control the final annealed structures and thus potentially the OCM activity and selectivity. Active OCM components that are nano-confined by the initial core–shell structures can be prepared. The step-by-step preparation of core–shell particles and improvement of the OCM activity are discussed in this paper.

2. Methods

2.1. Materials

All chemicals were used without further purification. Sodium tungstate dihydrate ($Na_2WO_4 \cdot 2H_2O$) was purchased from Yakuri Pure Chemicals (Kyoto, Japan). Potassium permanganate ($KMnO_4$, 99.3%) was purchased from Daejung Co., Ltd. (Siheung, Korea). Manganese acetate tetrahydrate [$Mn(CH_3CO)_2 \cdot 4H_2O$, 99.99%] was purchased from Sigma-Aldrich (St. Louis, Missouri, USA). Silica gel (SiO_2, 70–230 mesh, 99.5%) was purchased from Alfa Aesar (Haverhill, Massachusetts, USA). The TEOS [$Si(OC_2H_5)_4$] was purchased from Sigma-Aldrich (St. Louis, Missouri, USA). Aqueous ammonia solution (NH_3 (aq), 28.0–30.0%) was purchased from Sigma-Aldrich (St. Louis, Missouri, USA). Methane (99.5%), oxygen (99.95%), and nitrogen (99.9%) were purchased from Shinyang Sanso (Seoul, Korea). Deionized (DI) water (18.2 MΩ m) was prepared using an aquaMAX-Ultra 370 series water purification system (Young Lin Instruments, Anyang, Korea).

2.2. Preparation of supported powder catalysts

The mixed slurry method was used to prepare $Na_2WO_4/Mn/SiO_2$ catalysts with 5 wt% Na_2WO_4 and 2 wt% Mn supported by SiO_2.[23] A silica gel support (28 g) was mixed with DI water (150 mL) and stirred at 105 °C for 1 h. The $Mn(NO_3)_2 \cdot 6H_2O$ (1.8 mL) dissolved in DI water (10 mL) and $Na_2WO_4 \cdot 2H_2O$ (1.684 g) dissolved in DI water (10 mL) were drop-wise added to the boiling mixture for 15 min using a syringe pump. The generated thick paste was dried in air at 105 °C for 16 h and then calcined in air at 800 °C for 5 h. Prior to the reaction, the catalyst powder was sieved using a 150–250 mesh. Using the same procedure, additional catalysts were prepared by adding $KMnO_4$ or $Mn(CH_3CO)_2 \cdot 4H_2O$.

2.3. Preparation of SiO_2 spheres

The silica spheres used as cores were prepared using the Stöber method.[24–26] For this purpose, TEOS (30 mL) was hydrolysed in ethanol (170 mL) in the presence of aqueous ammonia solution (190 mL) and DI water (10 mL). The solvent was uniformly mixed using an impeller and added using a separatory funnel to hydrolyse the TEOS at a constant rate. The obtained silica spheres were washed with DI water and ethanol, centrifuged in a suspension, and dried in an oven at 80 °C for 24 h.

2.4. Preparation of $SiO_2@MnO_x$

The Mn species were deposited on the silica spheres ($SiO_2@MnO_x$) using a hydrothermal method. To prepare $SiO_2@Mn_xO_y$, the silica spheres (0.3 g) were dispersed in DI water (20 mL) at 30 °C for 1 h using ultrasonication,[27] followed by the addition of $KMnO_4$ (0.015–1.8 g) or $Mn(CH_3CO)_2 \cdot 4H_2O$ (or Mn-acetate, 0.15–1.8 g). Subsequently, the suspension was transferred to a Teflon-lined stainless-steel autoclave-type reactor and heated to 150 °C at a heating rate of 10 °C min^{-1}; the temperature was maintained at 150 °C for 48 h.[28–30] The autoclave-type reactor was then cooled to room temperature under ambient conditions. Subsequently, the $SiO_2@MnO_x(KMnO_4)$ and $SiO_2@MnO_x$(Mn-acetate) core–shell structures were collected by centrifugation and washed five times or more with ethanol and DI water. Potassium ions were removed by washing the core–shell structures.

2.5. Preparation of $SiO_2@MnO_x@Na_2WO_4$

The Na_2WO_4 was deposited on $SiO_2@MnO_x$ by drying an aqueous Na_2WO_4 solution in an oil bath. The $Na_2WO_4 \cdot 2H_2O$ (0.012 g) dissolved in DI water (15 mL) was stirred for 30 min at room temperature. The $SiO_2@MnO_x$ (0.2 g) was added to the mixture, which then was stirred for an hour. The suspension was transferred to an oil bath preheated to 105 °C and stirred until the water solvent was completely evaporated. The prepared powder was dried in air at 80 °C for 6 h to completely remove any moisture.

2.6. Preparation of $SiO_2@MnO_x@Na_2WO_4@SiO_2$ core–shell structures

Nanostructured core–shell catalysts with three shell layers composed of the active components of the OCM catalyst were synthesized. First, the TEOS was hydrolysed using the Stöber method to fabricate silica spheres with sizes between 600–800 nm, which were used as cores. Subsequently, two manganese precursors were selected, and the silica spheres were coated with the MnO_x shells using hydrothermal synthesis in a Teflon-lined stainless-steel autoclave. To attach Na_2WO_4 to the surface of the prepared $SiO_2@MnO_x$, DI water, $Na_2WO_4 \cdot 2H_2O$, and $SiO_2@MnO_x$ were added, followed by heating and stirring. Finally, the same method was used to fabricate silica spheres for the silica coating on the outermost layer of the catalyst.

2.7. Characterization of nanomaterials

Scanning electron microscopy (SEM) images of the catalysts were obtained using a Nova Nano SEM 200 instrument (FEI, Hillsboro, Oregon, USA). High-angle annular dark-field scanning transmission electron microscopy (HAADF-STEM) images of the catalysts were obtained using a Talos F200X instrument (FEI, Hillsboro, Oregon, USA). Both analyses were performed at the Korea Institute of Science and Technology (KIST) Advanced Analysis Center (Seoul, Korea). XRD results were collected using a Shimadzu XRD-6000 device equipped with a CuKα_1 (λ = 0.15406 nm) source.

2.8. Catalytic activity measurement

The catalytic reaction was performed in a fixed bed reactor. The outlets and inlets of the quartz reactor had the same size (internal diameter = 6 mm, external diameter = 8 mm). The catalyst bed was in the center of the reactor and the quartz wool was placed in the upper and lower layers of the catalyst bed. To minimize any homogeneous reactions, $ZrSiO_4$ beads (Cenotec, Co., Ltd.) were

added to the quartz reactor. The CH_4 and O_2 reactants diluted with N_2, flowed to the catalyst bed with each gas flow was controlled by a mass flow controller (MFC). The catalyst bed was primed with a N_2 flow for 30 min prior to the reaction. Water produced during the OCM reaction was removed using a cold trap connected to a −2 °C chiller (Jeio Tech, VTRC-620) and the CH_4, O_2, N_2, CO, CO_2, and hydrocarbons were analysed using the methanizer-equipped-flame ionization detector (FID), thermal conductivity detector (TCD) and FID of online gas chromatograph (GC, Agilent 7890A with ShinCarbon ST GC Columns (micropacked, RESTEK, 100/120 mesh, 2 m, 80 psi) was used to detect hydrocarbons. The catalysis results were calculated as follows:

$$C_{2+}\ \text{selectivity}\ (\%) = \frac{2 \times \text{moles of ethane and ethylene} + 3 \times \text{moles of propane and propylene}}{\text{moles of } CH_4 \text{ consumed}} \times 100$$

$$C_{2+}\ \text{yield}\ (\%) = \frac{2 \times \text{moles of ethane and ethylene} + 3 \times \text{moles of propane and propylene}}{\text{moles of } CH_4 \text{ in the feed}} \times 100$$

$$CH_4\ \text{conversion}\ (\%) = \frac{\text{moles of } CH_4 \text{ consumed}}{\text{moles of } CH_4 \text{ in the feed}} \times 100$$

The standard deviations of measured CH_4 conversion and C_{2+} selectivity were less than 5 and 3%, respectively.

3. Results and discussion

3.1. Preparation of SiO_2@MnO_x particles

Prior to the fabrication of core–shell particles, silica spheres with diameters of 600–800 nm (Fig. 1) were prepared using the Stöber method.[24–26] The SiO_2@MnO_x (Mn oxide shell deposited on SiO_2 spheres) was prepared by the deposition of MnO_x on the cores of the silica spheres. The MnO_x was deposited with a hydrothermal method utilizing $KMnO_4$ and $Mn(CH_3CO)_2 \cdot H_2O$ (Mn-acetate) as Mn species precursors.[28,29] The morphologies of the Mn shells differ depending on the Mn precursors. When $KMnO_4$ was used, plate-like shells formed on the surfaces of silica spheres. The morphology depends on the concentration of $KMnO_4$; the $(KMnO_4)/(SiO_2)$ ratio ranged from 0.02 to 2.22 (mol/mol). At a $(KMnO_4)/(SiO_2)$ ratio of 0.02–0.76 (mol/mol), SiO_2, the spheres were not completely covered with Mn species. However, they were completely covered at a $(KMnO_4)/(SiO_2)$ ratio of 1.52 (mol/mol) or higher. The Mn species, which completely cover the SiO_2 spheres, form nanoplate-like structures with a complex morphology that are stacked on top of each other (Fig. 2(f–h)). The transmission electron microscopy (TEM) images and energy dispersive X-ray spectroscopy (EDS) maps of SiO_2@MnO_x($KMnO_4$) confirm the deposition of nanoplate-like Mn species on the SiO_2 spheres and formation of Mn shells on SiO_2 spheres (Fig. 2(i–l)), respectively.

In addition to KMnO4, Mn-acetate was added to the silica spheres. The Mn-acetate forms shells on the silica spheres and Mn oxide nanowires (not deposited on the silica surface; Fig. 3(a–f)). Interestingly, the EDS maps indicate the formation of yolk–shell-like structures, creating empty space between the MnO_x shells and silica spheres (Fig. 3(g and h)).

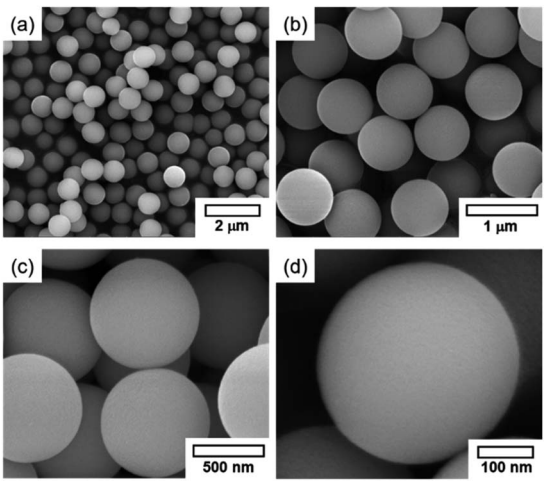

Fig. 1 SEM images of silica spheres prepared using the Stöber method.

3.2. Preparation of SiO_2@MnO_x@Na_2WO_4

The Na_2WO_4 was added to SiO_2@MnO_x($KMnO_4$) and SiO_2@-MnO_x(Mn-acetate). The deposition of Na_2WO_4 was analysed using EDS maps (Fig. 4). The morphology of SiO_2@MnO_x@-Na_2WO_4 insignificantly differs from that of SiO_2@MnO_x. These observations indicate the Na_2WO_4 deposition in the empty space between the MnO_x nanosheets and stabilization of Na_2WO_4 by MnO_x shells. The roughness of the MnO_x shells improves the deposition of Na_2WO_4 (Fig. 2 and 3). Note that Na_2WO_4 could not be deposited on the silica spheres without Mn species when a mixture of aqueous Na_2WO_4 solution and silica spheres was used, which indicates that it is difficult to deposit Na_2WO_4 on the silica surface and that an interaction between Na_2WO_4 and MnO_x is required for the formation of a Na_2WO_4 layer.

3.3. Preparation of SiO_2@MnO_x@Na_2WO_4@SiO_2

The SiO_2@MnO_x@Na_2WO_4@SiO_2 core–shell catalyst was prepared by forming a silica shell on SiO_2@MnO_x@Na_2WO_4

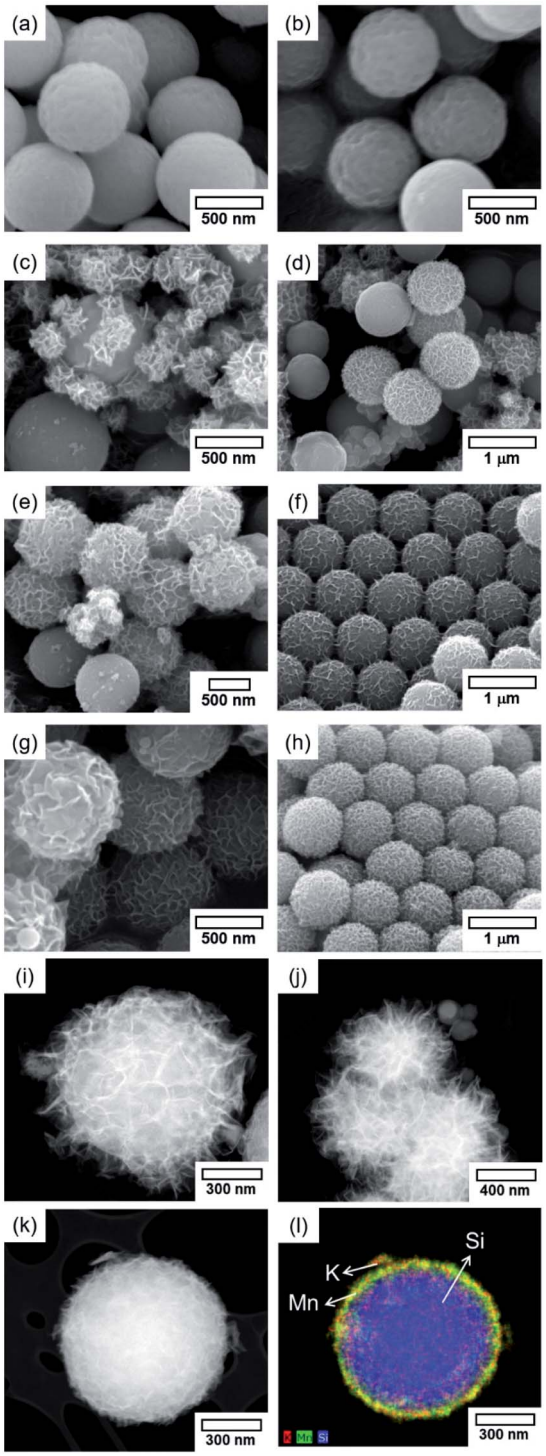

Fig. 2 SEM images of SiO_2@MnO_x($KMnO_4$) with ($KMnO_4$)/(SiO_2) ratios of (a) 0.02, (b) 0.04, (c) 0.38, (d) 0.57, (e) 0.76, (f) 1.52, (g) 1.90, and (h) 2.22 (mol/mol). (i and j) HAADF-STEM images of SiO_2@MnO_x($KMnO_4$) with a ($KMnO_4$)/(SiO_2) ratio of 2.22 (mol/mol). (k) HAADF-STEM images and (l) EDS maps of SiO_2@MnO_x($KMnO_4$) with a ($KMnO_4$)/(SiO_2) ratio of 0.19 (mol/mol).

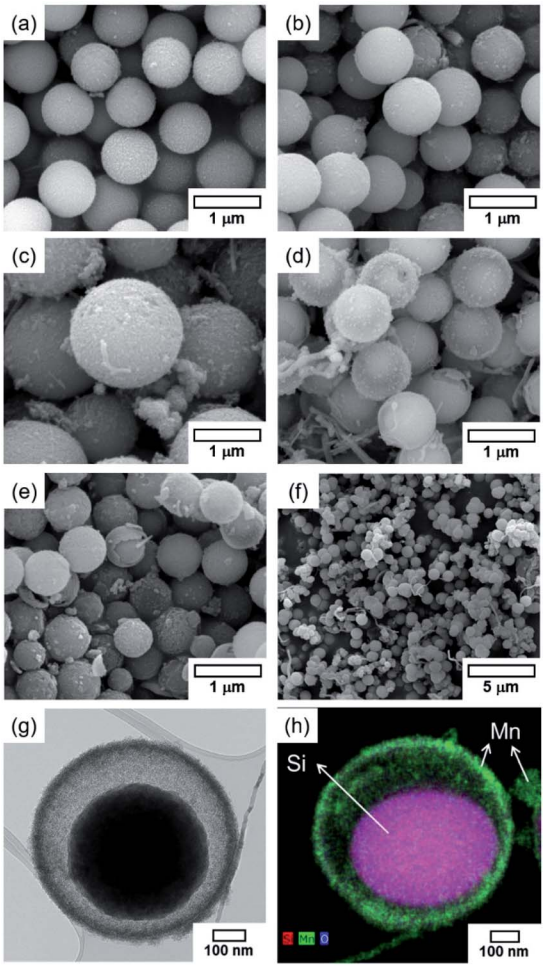

Fig. 3 SEM images of SiO_2@MnO_x(Mn-acetate) with (Mn-acetate)/(SiO_2) ratios of (a) 0.12, (b) 0.24, (c) 0.49, (d) 0.73, (e) 0.98, and (f) 1.47 (mol/mol). (g) TEM images and (h) EDS maps of SiO_2@MnO_x(Mn-acetate) with a (Mn-acetate)/(SiO_2) ratio of 0.73 (mol/mol).

(Fig. 5 and S1†). The thickness of the top SiO_2 shell was controlled by changing the quantity of tetraethyl orthosilicate (TEOS) precursors that were added to SiO_2@MnO_x@Na_2WO_4. Regarding the SiO_2@MnO_x($KMnO_4$)@Na_2WO_4@SiO_2 catalyst, the top shell of SiO_2 forms a rough surface, mimicking the surface morphology (Na_2WO_4 layer) of SiO_2@MnO_x($KMnO_4$)@Na_2WO_4. With increasing concentration of top-shell SiO_2, small SiO_2 particles (~100 nm) form, covering the surface of SiO_2@MnO_x($KMnO_4$)@Na_2WO_4. The EDS maps and TEM images indicate the formation of thin SiO_2 layers on the surface. Top-shell SiO_2 also forms on the surface of the SiO_2@MnO_x(Mn-acetate)@Na_2WO_4@SiO_2 catalyst. During the Mn-acetate deposition, isolated Mn rods form, which are also coated with SiO_2. The EDS maps and TEM images indicate that the deposition of SiO_2 insignificantly changes the core–shell structure of SiO_2@MnO_x(Mn-acetate)@Na_2WO_4.

3.4. OCM using core–shell structures

Core–shell catalysts prepared were used for the OCM (Fig. 6 and Table S1†). The OCM activity of SiO_2@MnO_x($KMnO_4$)@Na_2WO_4@SiO_2 was measured and compared with those of SiO_2@MnO_x($KMnO_4$)@Na_2WO_4 without outer SiO_2 shell, SiO_2@MnO_x(Mn-acetate)@Na_2WO_4@SiO_2, and conventional Na_2WO_4/Mn/SiO_2. Although SiO_2@MnO_x($KMnO_4$)

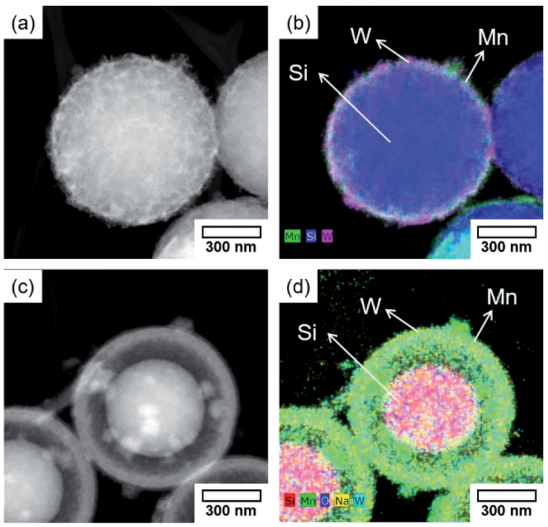

Fig. 4 HAADF-STEM images and EDS maps of (a and b) SiO_2@-$MnO_x(KMnO_4)$@Na_2WO_4 and (c and d) SiO_2@MnO_x(Mn-acetate) @Na_2WO_4.

@Na_2WO_4@SiO_2 was covered by the outer SiO_2 shell, it exhibited the slightly higher C_{2+} selectivity compared to Na_2WO_4/Mn/SiO_2 at 740–800 °C. SiO_2@MnO_x(Mn-acetate) @Na_2WO_4@SiO_2 exhibited poor OCM activity with lower CH_4 conversion and the lower C_{2+} selectivity which was confirmed by the EDS-STEM images (Fig. 7). SiO_2@$MnO_x(KMnO_4)$@Na_2WO_4 without the outer SiO_2 shell also exhibited lower CH_4 conversion (4.3–17.0%) compared to SiO_2@$MnO_x(KMnO_4)$@Na_2WO_4@SiO_2 (10.8–25.4%). The higher OCM activity of SiO_2@$MnO_x(KMnO_4)$@Na_2WO_4@SiO_2 compared to that of SiO_2@$MnO_x(KMnO_4)$@Na_2WO_4 without the outer SiO_2 shell can be attributed to the better dispersed Na_2WO_4 and MnO_x mixed with the outer SiO_2 shell as depicted in the EDS-STEM images (Fig. 7). With increasing gas hourly space velocity (GHSV) or decreasing contact time, CH_4 conversion decreased, and the C_{2+} selectivity slightly increased (Table S2†). The long term stability of SiO_2@$MnO_x(KMnO_4)$@Na_2WO_4@SiO_2 was also observed, as a stable C_{2+} yield was observed for up to 100 h. That said, the C_{2+} selectivity decreased slightly up to 20 h and remained stable thereafter (Fig. S2†).

The TEM results confirm that core–shell SiO_2@MnO_x@-Na_2WO_4@SiO_2 catalysts were successfully fabricated (Fig. 1–5). While the use of Mn as an oxygen supplier for the OCM reaction has been suggested,[16] Mn is also required for the production of well-dispersed Na_2WO_4 on Mn-based nanosheets in the core–shell structures. The formation of Mn-based nanosheets on the silica core spheres could be clearly observed when the $KMnO_4$ precursor was used. The better catalytic activity of SiO_2@-$MnO_x(KMnO_4)$@Na_2WO_4@SiO_2 can be attributed to the deposition of well-dispersed of Na_2WO_4 on Mn-based nanosheets. At high OCM reaction temperatures, the core–shell structure of SiO_2@$MnO_x(KMnO_4)$@Na_2WO_4@SiO_2 collapses into a complex SiO_2, MnO_x, and Na_2WO_4 composite. The successful OCM activity of collapsed SiO_2@$MnO_x(KMnO_4)$@Na_2WO_4@SiO_2 can be attributed to the formation of well-dispersed Na_2WO_4 particles on the Mn-bearing SiO_2 surface, which was derived from

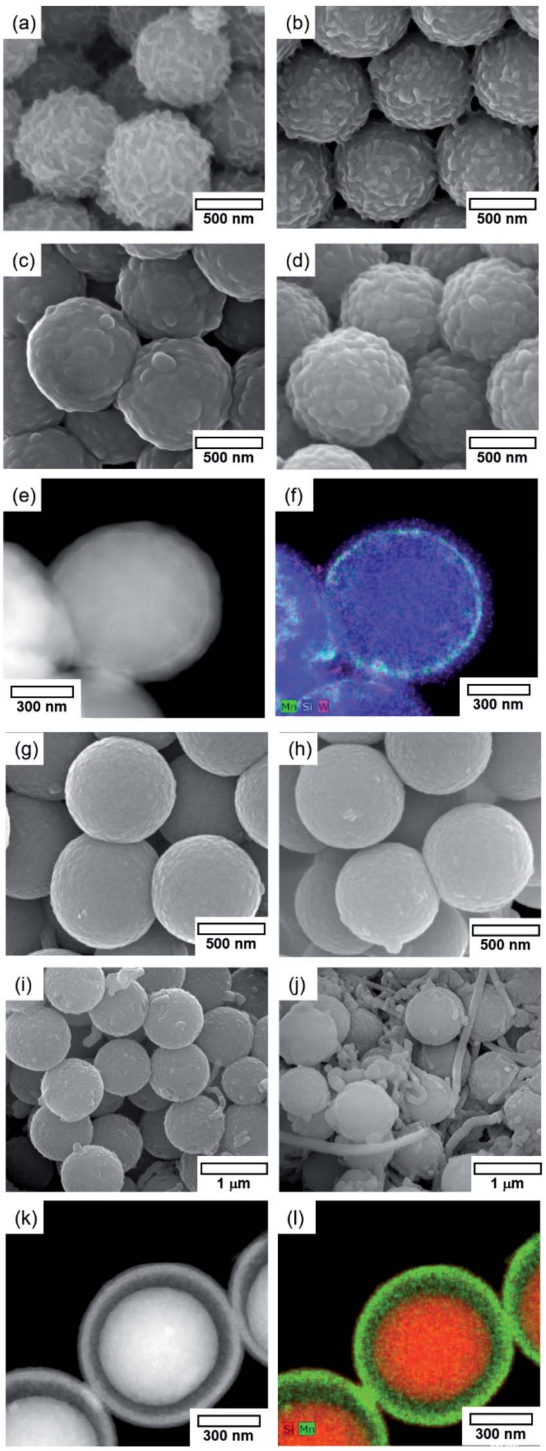

Fig. 5 SEM images of SiO_2@$MnO_x(KMnO_4)$@Na_2WO_4@SiO_2 with (SiO_2 core)/($KMnO_4$)/(Na_2WO_4)/(top-shell SiO_2) ratios of (a) 1/2.28/0.01/0.03, (b) 1/2.28/0.01/0.07, (c) 1/2.28/0.01/0.14, and (d) 1/2.28/0.01/0.29 (in mol) and SiO_2@MnO_x(Mn-acetate)@Na_2WO_4@SiO_2 with (SiO_2 core)/(Mn-acetate)/(Na_2WO_4)/(top-shell SiO_2) ratios of (g) 1/0.24/0.01/0.03, (h) 1/0.24/0.01/0.07, (i) 1/0.73/0.01/0.14, and (j) 1/1.47/0.01/0.29 (in mol). HAADF-STEM images and EDS maps of (e and f) SiO_2@$MnO_x(KMnO_4)$@Na_2WO_4@SiO_2 and (k and l) SiO_2@MnO_x(Mn-acetate)@Na_2WO_4@SiO_2.

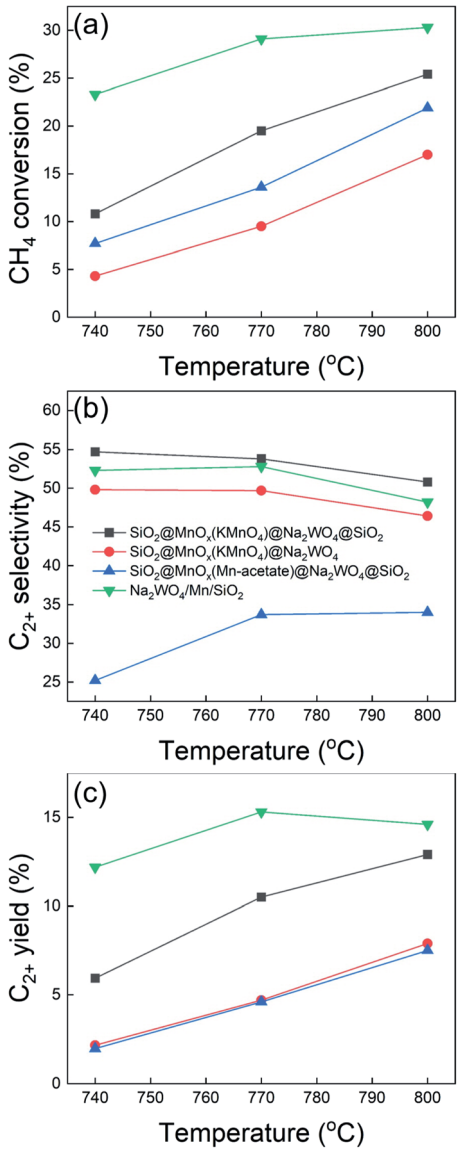

Fig. 6 Results of oxidative coupling of methane using core–shell catalysts. GHSV = 20 000 h^{-1}, $CH_4/O_2/N_2$ = 3/1/1 mol/mol/mol.

the initial core–shell structure. Core–shell structures and highly disperse catalysts are more selective with respect to the formation of C_{2+} compounds because of the confined Na_2WO_4 structure. Interestingly, $SiO_2@MnO_x$(Mn-acetate)$@Na_2WO_4@SiO_2$ exhibited spherical core–shell structures at high reaction temperature, despite being fully covered by the outer SiO_2 shell which suppressed the OCM reaction.

The XRD measurements indicate that the formation of α-cristobalite SiO_2 was observed for $SiO_2@MnO_x(KMnO_4)@Na_2WO_4@SiO_2$ and Na_2WO_4/Mn/SiO_2 but not for $SiO_2@MnO_x$(Mn-acetate)$@Na_2WO_4@SiO_2$ (Fig. 8). Because of the stabilizing effects of α-cristobalite SiO_2,[17] the poor OCM activity of $SiO_2@MnO_x$(Mn-acetate)$@Na_2WO_4@SiO_2$ can be attributed to the absence of α-cristobalite SiO_2. The formation of α-cristobalite SiO_2 for $SiO_2@MnO_x(KMnO_4)@Na_2WO_4@SiO_2$ indicated the formation of a complex mixture of Na_2WO_4 and the outer

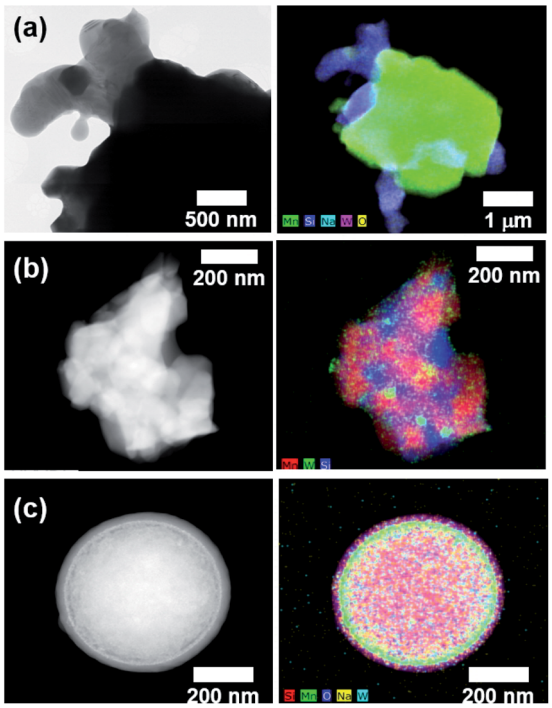

Fig. 7 HAADF-STEM images and EDS maps of (a) Na_2WO_4/Mn/SiO_2, (b) $SiO_2@MnO_x(KMnO_4)@Na_2WO_4@SiO_2$, and (c) $SiO_2@MnO_x$(Mn-acetate)$@Na_2WO_4@SiO_2$ after the OCM reaction.

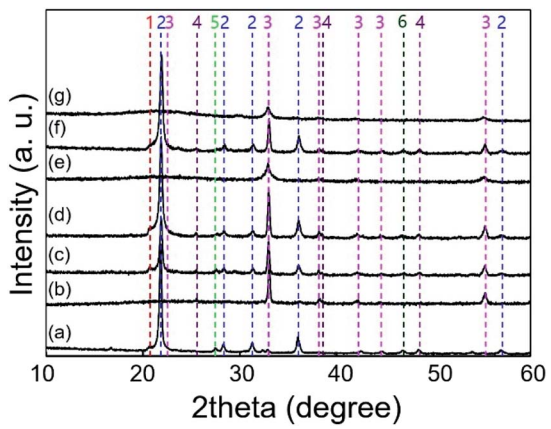

Fig. 8 XRD results of (a) Na_2WO_4/Mn/SiO_2, (b) $SiO_2@MnO_x(KMnO_4)$, (c) $SiO_2@MnO_x(KMnO_4)@Na_2WO_4$, (d) $SiO_2@MnO_x(KMnO_4)@Na_2WO_4@SiO_2$, (e) $SiO_2@MnO_x$(Mn-acetate), (f) $SiO_2@MnO_x$(Mn-acetate)$@Na_2WO_4$, and (g) $SiO_2@MnO_x$(Mn-acetate)$@Na_2WO_4@SiO_2$. All catalysts were fresh prior to the reaction. (1: tridymite, 2: α-cristobalite, 3: Mn_2O_3, 4: MnO_2, 5: Na_2WO_4, 6: $NaWO_3$).

SiO_2 shell because the permeation of Na into SiO_2 nucleated the α-cristobalite SiO_2.

The XPS exhibited distinct peaks of tungsten (W 4f) and sodium (Na 1s) for $SiO_2@MnO_x(KMnO_4)@Na_2WO_4@SiO_2$, but not for $SiO_2@MnO_x$(Mn-acetate)$@Na_2WO_4@SiO_2$ (Fig. 9). Because the OCM-active tungsten oxide was not clearly observed on the surface of $SiO_2@MnO_x$(Mn-acetate)$@Na_2WO_4@SiO_2$,[9,16,31,32] the OCM activity of $SiO_2@MnO_x$(Mn-acetate)$@Na_2WO_4@SiO_2$ was lower than those of other catalysts. These

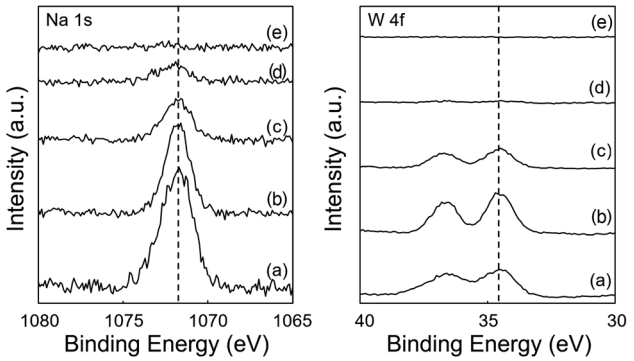

Fig. 9 Na 1s and W 4f XPS results of (a) $Na_2WO_4/Mn/SiO_2$, (b) $SiO_2@MnO_x(KMnO_4)@Na_2WO_4$, (c) $SiO_2@MnO_x(KMnO_4)@Na_2WO_4@SiO_2$, (d) $SiO_2@MnO_x$(Mn-acetate)$@Na_2WO_4$, and (e) $SiO_2@MnO_x$(Mn-acetate)$@Na_2WO_4@SiO_2$. All catalysts were fresh prior to the reaction.

observations can be attributed to the outer SiO_2 shell blocking the active tungsten oxide for $SiO_2@MnO_x$(Mn-acetate)$@Na_2WO_4@SiO_2$ as depicted in the EDS-STEM images. $SiO_2@MnO_x(KMnO_4)@Na_2WO_4@SiO_2$ exhibited appreciable W 4f peaks indicating exposed active sites for the OCM.

3.5. Reaction mechanism on the core–shell catalysts

$SiO_2@MnO_x(KMnO_4)@Na_2WO_4@SiO_2$ exhibited slightly higher C_{2+} selectivity compared to the conventional $Na_2WO_4/Mn/SiO_2$ catalyst although it was covered by the outer SiO_2 shell. The selective OCM activity can be attributed to the formation of a complex of Na_2WO_4, MnO_x, and SiO_2 as observed on the TEM, XRD, and Raman results. The presence of complex mixed oxides improved the dispersion of Na_2WO_4 in the mixture of MnO_x and SiO_2 selectively catalysing OCM.

4. Conclusion

In this study, $SiO_2@MnO_x@Na_2WO_4@SiO_2$ core–shell structures were prepared. Nanostructured shells of Mn oxide and Na_2WO_4 consecutively formed and were protected using SiO_2 sols. Although the complex core–shell structures were destroyed at a temperature of 700–800 °C at which the OCM to olefins and paraffins was performed, highly dispersed Na_2WO_4 on the MnO_x layer is derived from nanoscopic core–shell structures. The Na_2WO_4 may be confined to the complex structures of MnO_x and SiO_2. The catalyst derived from the core–shell Na_2WO_4–Mn–SiO_2 complex exhibits an improved production of C_{2+} compounds and the further oxidation of C_{2+} compounds to CO and CO_2 may be suppressed by highly dispersed Na_2WO_4.

Conflicts of interest

There are no conflicts to declare.

Acknowledgements

This work was supported by the C1 Gas Refinery Program of the National Research Foundation of Korea (NRF) funded by the Ministry of Science and ICT (2015M3D3A1A01064900).

Notes and references

1 R. T. Yunarti, S. Gu, J.-W. Choi, J. Jae, D. J. Suh and J.-M. Ha, *ACS Sustainable Chem. Eng.*, 2017, **5**, 3667–3674.
2 C. Hammond, S. Conrad and I. Hermans, *ChemSusChem*, 2012, **5**, 1668–1686.
3 H. R. Godini, S. Xiao, S. Jašo, S. Stünkel, D. Salerno, N. X. Son, S. Song and G. Wozny, *Fuel Process. Technol.*, 2013, **106**, 684–694.
4 Z. Zakaria and S. K. Kamarudin, *Renewable Sustainable Energy Rev.*, 2016, **65**, 250–261.
5 V. Paunović and J. Pérez-Ramírez, *Catal. Sci. Technol.*, 2019, **9**, 4515–4530.
6 Y. Gambo, A. A. Jalil, S. Triwahyono and A. A. Abdulrasheed, *J. Ind. Eng. Chem.*, 2018, **59**, 218–229.
7 T. Ito and J. H. Lunsford, *Nature*, 1985, **314**, 721–722.
8 G. E. Keller and M. M. Bhasin, *J. Catal.*, 1982, **73**, 9–19.
9 S. Arndt, T. Otremba, U. Simon, M. Yildiz, H. Schubert and R. Schomäcker, *Appl. Catal., A*, 2012, **425–426**, 53–61.
10 T. W. Elkins, B. Neumann, M. Bäumer and H. E. Hagelin-Weaver, *ACS Catal.*, 2014, **4**, 1972–1990.
11 G. Lee, I. Kim, I. Yang, J.-M. Ha, H. B. Na and J. C. Jung, *Appl. Surf. Sci.*, 2018, **429**, 55–61.
12 S. Lim, J.-W. Choi, D. J. Suh, K. H. Song, H. C. Ham and J.-M. Ha, *J. Catal.*, 2019, **375**, 478–492.
13 T. W. Elkins and H. E. Hagelin-Weaver, *Appl. Catal., A*, 2013, **454**, 100–114.
14 J. W. Xu, Y. Zhang, Y. M. Liu, X. Z. Fang, X. L. Xu, W. M. Liu, R. Y. Zheng and X. Wang, *Eur. J. Inorg. Chem.*, 2019, 183–194.
15 X. Fang, S. Li, J. Lin and Y. Chu, *J. Mol. Catal.*, 1992, **6**, 427–433.
16 S. Gu, H.-S. Oh, J.-W. Choi, D. J. Suh, J. Jae, J. Choi and J.-M. Ha, *Appl. Catal., A*, 2018, **562**, 114–119.
17 Z. C. Jiang, C. J. Yu, X. P. Fang, S. B. Li and H. L. Wang, *J. Phys. Chem.*, 1993, **97**, 12870–12875.
18 N. S. Hayek, G. J. Khlief, F. Horani and O. M. Gazit, *J. Catal.*, 2019, **376**, 25–31.
19 N. Hiyoshi and T. Ikeda, *Fuel Process. Technol.*, 2015, **133**, 29–34.
20 M. Yildiz, Y. Aksu, U. Simon, T. Otremba, K. Kailasam, C. Gobel, F. Girgsdies, O. Gorke, F. Rosowski, A. Thomas, R. Schomacker and S. Arndt, *Appl. Catal., A*, 2016, **525**, 168–179.
21 D. Sun, S. Wageh, A. A. Al-Ghamdi, Y. Le, J. Yu and C. Jiang, *Appl. Surf. Sci.*, 2019, **466**, 301–308.
22 Y.-F. Huang, X.-Y. Sun, S.-H. Huo, Y. Li and C. Zhong, *Appl. Surf. Sci.*, 2019, **466**, 637–646.
23 J. Y. Lee, W. Jeon, J.-W. Choi, Y.-W. Suh, J.-M. Ha, D. J. Suh and Y.-K. Park, *Fuel*, 2013, **106**, 851–857.
24 W. Stöber, A. Fink and E. Bohn, *J. Colloid Interface Sci.*, 1968, **26**, 62–69.
25 W. Li and D. Zhao, *Adv. Mater.*, 2013, **25**, 142–149.
26 X. Jiang, Y. Wang and M. Li, *Sci. Rep.*, 2014, **4**, 6070.
27 H. Shi, D. Shi, L. Yin, Z. Yang, S. Luan, J. Gao, J. Zha, J. Yin and R. K. Li, *Nanoscale*, 2014, **6**, 13748–13753.

28 D. Yuan, T. Zhang, Q. Guo, F. Qiu, D. Yang and Z. Ou, *Chem. Eng. J.*, 2017, **327**, 539–547.
29 D. Kong, M. Yu, C. Lin, X. Liu, J. Lin and J. Fang, *J. Electrochem. Soc.*, 2005, **152**, H146–H151.
30 M. Qiao, X. Lei, Y. Ma, L. Tian, W. Wang, K. Su and Q. Zhang, *J. Alloys Compd.*, 2017, **693**, 432–439.
31 Y. Kou, B. Zhang, J.-z. Niu, S.-b. Li, H.-l. Wang, T. Tanaka and S. Yoshida, *J. Catal.*, 1998, **173**, 399–408.
32 S.-B. Li, *Chin. J. Chem.*, 2001, **19**, 16–21.